

Article

Effect of Preparation Method on ZrO₂-Based Catalysts Performance for Isobutanol Synthesis from Syngas

Yingquan Wu ¹, Li Tan ^{2,3,*}, Tao Zhang ¹, Hongjuan Xie ¹, Guohui Yang ¹, Noritatsu Tsubaki ³ and Jiangang Chen ¹

¹ State Key Laboratory of Coal Conversion, Institute of Coal Chemistry, Chinese Academy of Sciences, Taiyuan 030001, China

² Institute of Molecular Catalysis and Operando Characterization, College of Chemistry, Fuzhou University, Fuzhou 350108, China

³ Department of Applied Chemistry, University of Toyama, Toyama 930-8555, Japan

* Correspondence: tan@fzu.edu.cn; Tel.: +86-186-3698-4914

Received: 15 July 2019; Accepted: 3 September 2019; Published: 6 September 2019



Abstract: Two types of amorphous ZrO₂ (am-ZrO₂) catalysts were prepared by different co-precipitation/reflux digestion methods (with ethylenediamine and ammonia as the precipitant respectively). Then, copper and potassium were introduced for modifying ZrO₂ via an impregnation method to enhance the catalytic performance. The obtained catalysts were further characterized by means of Brunauer-Emmett-Teller surface areas (BET), X-ray diffraction (XRD), H₂-temperature-programmed reduction (H₂-TPR), and In situ diffuse reflectance infrared spectroscopy (in situ DRIFTS). CO hydrogenation experiments were performed in a fixed-bed reactor for isobutanol synthesis. Great differences were observed on the distribution of alcohols over the two types of ZrO₂ catalysts, which were promoted with the same content of Cu and K. The selectivity of isobutanol on K-CuZrO₂ (ammonia as precipitant, A-KCZ) was three times higher than that on K-CuZrO₂ (ethylenediamine as precipitant, E-KCZ). The characterization results indicated that the A-KCZ catalyst supplied more active hydroxyls (isolated hydroxyls) for anchoring and dispersing Cu. More importantly, it was found that bicarbonate species were formed, which were ascribed as important C₁ species for isobutanol formation on the A-KCZ catalyst surface. These C₁ intermediates had relatively stronger adsorption strength than those adsorbed on the E-KCZ catalyst, indicating that the bicarbonate species on the A-KCZ catalyst had a longer residence time for further carbon chain growth. Therefore, the selectivity of isobutanol was greatly enhanced. These findings would extend the horizontal of direct alcohols synthesis from syngas.

Keywords: preparation method; ZrO₂-based catalysts; syngas; isobutanol

1. Introduction

Higher alcohols (C₂₊ alcohols) synthesized from syngas have been studied owing to their broad applications [1–5]. Higher alcohol isobutanol has been extensively used as an important organic chemical raw material to manufacture plasticizers (diisobutyl phthalate), adhesives, isobutylene isoprene rubber, and antioxidants, among others. Isobutanol is also used in advanced solvents to purify special chemicals, such as salts of strontium, barium, and lithium. Furthermore, isobutanol can be added to gasoline as a fuel additive, which not only increases the octane number, but also reduces carbon monoxide, nitrogen oxides, and hydrocarbon emissions in exhaust gas.

Presently, there is no industrialized method for the direct synthesis of isobutanol. The main source of isobutanol is as a by-product from the carbonylation of propylene to *n*-butanol. This low yield of isobutanol is far from meeting the increasing market demand. In recent years, increasing

studies have focused on direct routes for the synthesis of higher alcohols synthesis from syngas. As a vital chemical among higher alcohols, the direct synthesis of isobutanol from syngas has been extensively studied. Typically, three main catalytic systems have been used, namely, ZnCr [6–8], CuZnAl [9–11], and ZrO₂ catalysts [12–14]. Typical isobutanol yields reported in the literature are shown in Table 1. Zirconia oxides promoted by other components (such as K, Pd, and Cu) have been reported as effective catalysts for the direct synthesis of isobutanol from syngas. Zirconia-based catalysts have been studied extensively, including the effects of catalyst composition, various promoters, reaction conditions, and ZrO₂ crystal phase structures on isobutanol formation. Wang et al. [15] found that tetragonal ZrO₂ (t-ZrO₂) favored isobutanol production. He et al. [13] found that the ZrO₂ with a surface tetragonal crystal phase (t-ZrO₂) exhibited high activity for ethanol formation, while ZrO₂ with a surface monoclinic crystal phase (m-ZrO₂) exhibited high activity for isobutanol formation. In a previous study [14], we found that amorphous ZrO₂ promoted isobutanol synthesis. These results show that the distribution of alcohols is closely related to the ZrO₂ crystalline phase. Further reports [16,17] have shown that when the same amount of copper is loaded onto different ZrO₂ crystalline phases, the catalysts show distinctly different catalytic activities. The catalyst Cu/m-ZrO₂ exhibited better activity than Cu/t-ZrO₂ in the synthesis of methanol from H₂/CO. This difference in activity was attributed to the different hydroxyl properties on the carrier surface.

Table 1. Representative isobutanol synthesis catalysts.

Catalyst	T (°C)	P (MPa)	CO/H ₂	GHSV (h ⁻¹)	Isobutanol (wt%)
K-Zn ₁ Cr ₁ [6]	400	10	2.5	3000	15.99
Cr/ZnO-K [7]	400	10	2.3	3000	15.58
K-Zn ₁ Cr ₁ (pH = 2) [8]	400	10	2.5	3000	24.2
Cu/ZnO/Al ₂ O ₃ /30% ACFs [9]	320	4	2	3900	19.88
K-CuZrAl [10]	400	10	2.7	5000	17.7
K-ZrO ₂ [12]	420	10	2.1	5000	15.1
Li-Pd-ZrO ₂ [13]	400	8	2	15,000	23.1
K-CuLaZrO ₂ [14]	360	10	2.5	3000	32.8

Previously, Jackson et al. [18] investigated the source and role of oxygen in the formation of adsorbed species (such as carbonate and formate) and found that hydroxyl groups on the ZrO₂ surface participated in methanol formation. A formate-to-methoxide mechanism for methanol synthesis was then proposed. Tian et al. [19] studied the adsorption of CO on ZnCr catalyst using in-situ infrared spectroscopy, finding that a large number of formed formate species were consumed after hydroxyl groups were adsorbed on the catalyst surface. This indicated that hydroxyl groups promoted the formation of C₁ species (HCOO⁻), which are important intermediates for alcohol synthesis. Gao et al. [8] also found that the formation of formate species was related to surface hydroxyl groups. Meanwhile, oxygen vacancies, as active sites for CO activation, could be formed after removing -OH using CO. Therefore, hydroxyl groups on the catalyst surface play an important role in the synthesis of higher alcohols from syngas.

Owing to the different crystalline phases of ZrO₂, the type and content of hydroxyl groups on the catalyst surface are different, while the amount of CO adsorption on the catalyst surface is also different. However, the main reason for the different product distributions of isobutanol over different ZrO₂ crystalline phases remains unclear, owing to the complexity of the conversion of syngas to isobutanol. Therefore, to further study the factors influencing isobutanol synthesis, in the present study, two types of amorphous ZrO₂ were prepared by different preparation methods and then loaded with the same amounts of Cu and K, which aided isobutanol synthesis [19,20]. Finally, these catalysts were applied to isobutanol synthesis from syngas. The results showed that although all catalysts were amorphous ZrO₂, the distribution of alcohol products varied greatly. To understand the relationship between the catalyst surface properties, especially the hydroxyl groups on the catalyst surface, and the isobutanol formation process, in-situ DRIFTS was used to investigate the hydroxyl groups and C₁ intermediates

on the surfaces of different catalysts. The types and contents of hydroxyl groups on the catalyst surface varied greatly, which led to changes in the types and contents of adsorbed species, ultimately resulting in the formation of different reaction products. Herein, the mechanism of isobutanol synthesis from syngas was further studied, resulting in important findings that will broaden the scope of direct alcohols synthesis from syngas and the design of alcohol synthesis catalysts.

2. Results and Discussions

2.1. Catalytic Performance

The catalytic performance of ZrO₂-based catalysts in isobutanol synthesis from CO hydrogenation at 350 °C and 10.0 MPa for 3000 h⁻¹ is shown in Table 2. The results showed that all ZrO₂-based catalysts catalyzed CO hydrogenation to higher alcohols. However, different distributions of alcohols were obtained using different catalysts. Alkanes were the main products on the E-ZrO₂ catalyst, while the selectivity for alcohols was only 14.5%. Among alcohols, methanol was the primary product, with only 5.4% selectivity observed for C₂₊ alcohols. Adding potassium and copper significantly improved the activity of the ZrO₂ catalysts for higher alcohols synthesis, with CO conversion over the E-KCZ catalyst increasing dramatically to 37.7% compared with 10.9% for that without K and Cu, while the space-time yield (STY) of alcohols also increased from 34 to 144 g·L⁻¹·h⁻¹. Alkane formation was inhibited, leading to an increase in alcohol selectivity. In the isobutanol synthesis reaction, CO₂ was also detected owing to the water-gas-shift (WGS) reaction. The selectivity for methanol decreased from 94.6% to 90.0%, while the selectivity for isobutanol increased from 0.5% to 4.7%. When the Gas Hour Space Velocity (GHSV) was increased to 7000 h⁻¹, the CO conversion decreased to 14.5%. The alcohols STY and selectivity for all alcohols clearly increased, while the selectivities for CH_x, CO₂, and dimethyl ether (DME) were decreased to varying degrees. The selectivity for isobutanol among alcohol products also decreased to 3.2%. The distribution of products from the A-ZrO₂ catalyst was similar to that from the E-ZrO₂ catalyst. Adding K and Cu also clearly promoted the activity of the A-ZrO₂ catalyst, with the CO conversion increasing from 13.2% to 41.2%, while the alcohols STY increased from 24 to 195 g·L⁻¹·h⁻¹. Among alcohols, methanol was the major product using the A-ZrO₂ catalyst. However, methanol and isobutanol became the primary products after activity promotion by K and Cu. The selectivity of isobutanol increased from 0.8% to 15.0%. A high GHSV (7000 h⁻¹) also caused a significant decrease in CO conversion, with the selectivity for isobutanol decreasing to 10.2%. As the GHSV increased, the isobutanol formation process became more difficult owing to the shorter time for carbon chain growth. Based on the results above, the alcohol distributions obtained using two types of ZrO₂-based catalyst were very different, and were promoted by the same elements. Therefore, the properties of the two types of ZrO₂ catalysts required further investigation. The stability of the A-KCZ catalyst is shown in Figure 1. The A-KCZ catalyst showed excellent stability over 84 h on stream. The isobutanol selectivity was stably maintained at around 14 wt% throughout the test. The CO conversion declined after the first 7 h and then showed no obvious change.

Table 2. The catalytic performance of ZrO₂-based catalysts.

Catalysts	CO Conv. (%)	Alc. STY (g·L ⁻¹ ·h ⁻¹)	Selectivity (C-atom%)				Alc. Distribution (wt%)				
			Alc.	CH _x	CO ₂	DME	C ₁	C ₂	C ₃	i-C ₄	C ₄₊
E-ZrO ₂	10.9	34	14.5	84.9	0	0.6	94.6	4.2	0.7	0.5	0
E-KCZ	37.7	144	25.5	37.9	33.5	3.1	90.0	3.6	1.5	4.7	0.2
E-KCZ ^a	14.5	284	40.1	29.7	28.7	1.5	92.9	2.8	1.0	3.2	0.1
A-ZrO ₂	13.2	24	19.6	79.8	0	0.6	97.2	1.6	0.4	0.8	0
A-KCZ	41.2	195	42.3	31.1	25.4	1.2	78.8	2.7	2.1	15.0	1.4
A-KCZ ^a	16.8	315	56.2	24.6	18.2	1.0	86.0	2.2	0.9	10.2	0.7

Reaction conditions: K(2 wt%)-Cu(5 wt%)-ZrO₂, P = 10.0 MPa, GHSV = 3000 h⁻¹, Temperature = 350 °C, H₂/CO = 2.5/1. ^a GHSV = 7000 h⁻¹, P = 10.0 MPa, Temperature = 350 °C, H₂/CO = 2.5/1.

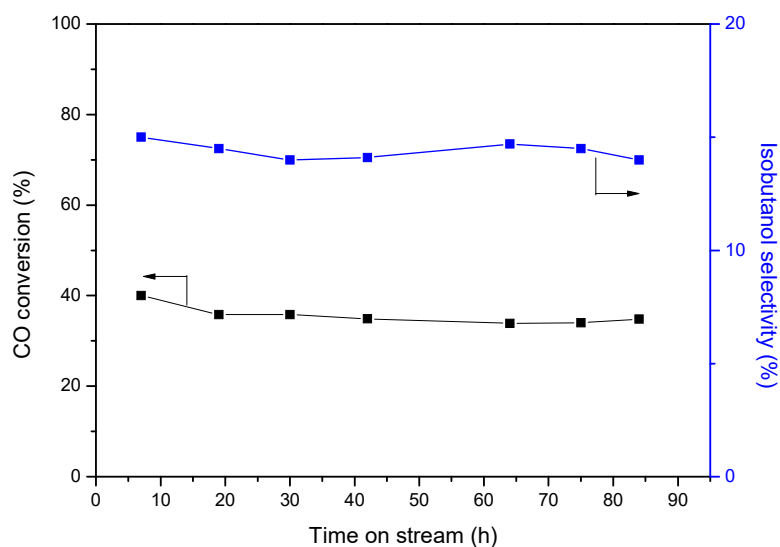


Figure 1. The stability of A-KCZ catalyst under reaction conditions (300 °C, 10 MPa, 3000 h⁻¹).

2.2. Textural Properties

The textural parameters of the fresh and reduced ZrO₂-based catalysts are shown in Table 3. Compared with the fresh A-ZrO₂ catalyst, a larger specific surface area was obtained on the fresh E-ZrO₂ catalyst. This increased specific surface area was accompanied by a decreased pore size. When K and Cu were introduced to promote ZrO₂ catalyst activity, the specific surface areas of both E-ZrO₂ and A-ZrO₂ decreased from 424.66 and 309.87 to 315.69 and 243.59 m²g⁻¹, respectively. After reduction, the specific surface area of all catalysts showed a slight increase. The Cu⁰ surface areas were also determined by N₂O reactive frontal chromatography, with the results shown in Table 2. The specific surface areas of Cu on A-KCZ and E-KCZ were almost identical. As the E-ZrO₂ catalyst had a higher specific surface area, it was speculated that Cu was better dispersed on the A-ZrO₂ catalyst.

Table 3. Textural properties of calcined catalysts.

Catalysts	Pore Diameter, nm	Pore Volume, cm ³ g ⁻¹	A _{BET} , m ² g ⁻¹	S _{Cu} (m ² /g)
E-ZrO ₂ ^a	5.80	0.62	424.66	-
A-ZrO ₂ ^a	9.10	0.71	309.87	-
E-KCZ ^a	6.91	0.55	315.69	11.6
A-KCZ ^a	9.66	0.59	243.59	11.3
E-ZrO ₂ ^b	5.65	0.63	430.85	-
A-ZrO ₂ ^b	9.01	0.77	313.54	-
E-KCZ ^b	6.88	0.55	320.80	-
A-KCZ ^b	9.89	0.68	273.24	-

^a fresh catalysts. ^b reduced catalysts.

2.3. Powder XRD Measurements

XRD patterns of the fresh and reduced ZrO₂-based catalysts synthesized by different methods are shown in Figure 2. As shown in Figure 2a, both the E-ZrO₂ and A-ZrO₂ catalysts exhibited a wide peak structure centered at ~31°, which was attributed to amorphous zirconia (am-ZrO₂) [21,22]. No diffraction peak related to the ZrO₂ crystal structure was observed. After adding K and Cu, the E-KCZ and A-KCZ catalysts possessed a broad peak centered at ~31°, indicating that ZrO₂ existed in an amorphous state. Meanwhile, no diffraction peaks for K₂O or CuO crystals were found in all catalysts, showing that K₂O and CuO were highly dispersed on ZrO₂, or existed in small crystals. When these catalysts were reduced by 10% H₂/N₂, no significant changes in the E-ZrO₂, E-ZrO₂, and

E-KCZ catalysts were observed, but a small amount of $t\text{-ZrO}_2$ appeared after the A-KCZ catalyst was reduced. This conversion into ZrO_2 crystals might be related to the decline in CO conversion during the first 7 h of reaction (Figure 1). No other diffraction peaks appeared, indicating that K_2O and Cu were well dispersed.

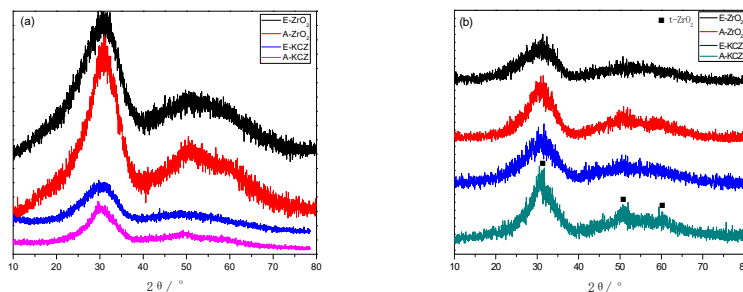


Figure 2. XRD patterns of ZrO_2 -based catalysts (a) fresh catalysts, (b) reduced catalysts.

2.4. H_2 -TPR Analysis

H_2 -TPR analysis was conducted to evaluate the reducibility of Cu species related to the active sites and to investigate the interaction between Cu and Zr (Figure 3). According to the H_2 -TPR results, both samples with 5 wt% Cu exhibited peaks between 200 and 260 °C. Generally, the reduction temperature of pure CuO is relatively high (around 320 °C) and only one single peak is observed [23]. In this study, a Cu- ZrO_2 interaction was concluded to be present, which aided the reduction of supported Cu elements. However, three hydrogen consumption peaks were observed on the E-KCZ catalyst, which were located at 217 °C (α), 231 °C (β), and 248 °C (γ). Similar results have been reported previously, with the lower-temperature peak attributed to the reduction of well-dispersed CuO or Cu^{2+} ions in an octahedral environment. Meanwhile, the higher-temperature peak has been attributed to the reduction of bulk CuO [24,25]. Therefore, the α peak is related to highly dispersed CuO, the β peak is related to CuO species interacting strongly with ZrO_2 , while the γ peak is related to the reduction of bulk CuO [23]. In contrast to the E-KCZ catalyst, the A-KCZ catalyst showed only one H_2 consumption peak. From the peak location, it was attributed to the reduction of CuO species interacting strongly with ZrO_2 . The H_2 -TPR results indicated that the dispersion of Cu species on two types of carrier was totally different. Cu species were well dispersed on the A- ZrO_2 catalyst, while having strong interactions with the carrier. In contrast, Cu species were not well dispersed on the E- ZrO_2 catalyst, leading to different Cu species, while E- ZrO_2 had a larger specific surface area than A- ZrO_2 . Therefore, these two types of carriers must have different surface properties.

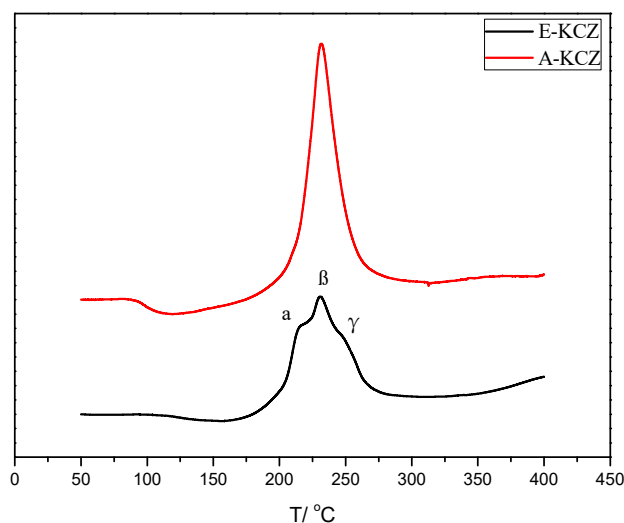


Figure 3. H_2 -TPR profiles of ZrO_2 -based catalysts.

2.5. Hydroxyl Groups on Different Catalysts

Figure 4 shows the hydroxyl region ($4000\text{--}3000\text{ cm}^{-1}$) of the infrared spectra obtained at $250\text{ }^{\circ}\text{C}$. Adsorbed water (or coordinated water) is known to be weakly adsorbed on the zirconia surface and desorbed by heating to $250\text{ }^{\circ}\text{C}$ under vacuum, while hydroxyl groups on the zirconia surface can exist stably even at $600\text{ }^{\circ}\text{C}$ under vacuum [26,27]. Therefore, all samples were pretreated in situ at $250\text{ }^{\circ}\text{C}$ under vacuum for 1 h to remove surface-adsorbed water before recording IR spectra, resulting in no peaks related to the presence of molecularly adsorbed water. In Figure 4, a band at 3732 cm^{-1} with a broad shoulder at about 3673 cm^{-1} was observed in the E-ZrO₂ catalyst. After copper and potassium impregnation (E-KCZ), the strength of the bands at 3732 cm^{-1} and 3673 cm^{-1} decreased obviously, while a new band located at 3726 cm^{-1} appeared as that at 3732 cm^{-1} decreased. Two absorption bands were observed for the A-ZrO₂ catalyst, located in the regions of 3732 and 3673 cm^{-1} , respectively. A shoulder peak at around 3755 cm^{-1} was also observed. When Cu and K were both introduced, a dramatic decrease in the peak intensities at 3755 , 3732 , and 3673 cm^{-1} was observed. A new peak located at 3715 cm^{-1} appeared after impregnation. Meanwhile, the broad peak between 3600 and 3000 cm^{-1} seems to slightly increase in intensity.

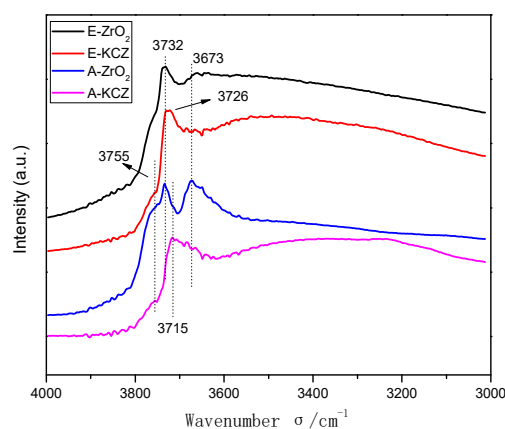


Figure 4. Infrared spectra of ZrO₂-based catalysts.

Generally, peaks in the $3800\text{--}3700\text{ cm}^{-1}$ region can be assigned to monocoordinated hydroxyl groups, those at $3700\text{--}3600\text{ cm}^{-1}$ can be assigned to bi-bridged hydroxyl groups, and those below 3600 cm^{-1} can be assigned to multicoordinated hydroxyl groups (hydrogen-bridged species) [28,29]. However, some researchers have proposed that peaks higher than 3650 cm^{-1} are related to the vibration of isolated --OH groups on the oxide [30–32]. The types of specific hydroxyl groups are more difficult to distinguish clearly. However, the E-ZrO₂ catalyst showed more multicoordinated hydroxyl groups, while the A-ZrO₂ catalyst showed more isolated surface hydroxyl groups.

Chen et al. [33] reported that the isolated hydroxyl groups on Al₂O₃ were active sites for anchoring Pt and Ni. The authors showed that the hydroxyl groups not only had an important effect on Pt and Ni dispersion, but also influenced the interactions between Pt and the support. A-ZrO₂ had more isolated surface hydroxyl groups, which led to a greater loss in intensity after Cu and K impregnation, indicating that A-ZrO₂ had more active --OH groups than the other catalysts. Therefore, Cu species were well dispersed on A-ZrO₂, which was consistent with the H₂-TPR results.

2.6. In Situ DRIFTS Analysis

The surface properties of catalysts were different according to the preparation method used. In-situ DRIFTS was used to study the adsorption and activation of syngas molecules on different catalyst surfaces at the reaction temperature. Figure 5 shows spectra recorded after saturated CO adsorption. On E-ZrO₂, a broad negative peak at around 3500 cm^{-1} appeared with CO adsorption, indicating that surface --OH groups were consumed by CO, especially the isolated hydroxyl groups.

Interestingly, a small peak located at 3739 cm^{-1} also appeared after CO adsorption, for which the cause remains unclear, although it might be attributed to the decomposition of multicoordinated hydroxyl groups. The absorption bands observed at 2967 ($\nu_{\text{SCOO}^-} + \delta_{\text{CH}}$), 2884 (ν_{CH}), 1576 (ν_{asCOO^-}), 1388 (δ_{CH}), and 1370 cm^{-1} (ν_{SCOO^-}) were attributed to bidentate formate species (b-HCO_3^-) on E-ZrO₂ [34–36]. The peaks located at 2178 and 2116 cm^{-1} were attributed to the vibration of gaseous CO. A small amount of CO₂ (2364 and 2337 cm^{-1}) was also observed. The adsorption species on A-ZrO₂ were similar to those on E-ZrO₂, with bidentate formate as the main species. However, a difference in the consumption of –OH groups was observed. In addition to the isolated hydroxyl groups, multicoordinated hydroxyl groups were also consumed owing to the appearance of negative peaks at lower wave numbers ($<3600\text{ cm}^{-1}$). Isolated hydroxyl groups were proposed to react readily with CO to form formate species [37]. A-ZrO₂ had more isolated surface hydroxyl groups, resulting in more formate species on A-ZrO₂ compared with that on E-ZrO₂, as determined from the different peak intensities. Formate species are recognized as a C₁ intermediate in methanol synthesis from syngas [38–40]. Therefore, methanol was the main alcohol product (Table 2) because formate species were the main intermediates on both E-ZrO₂ and A-ZrO₂ catalysts.

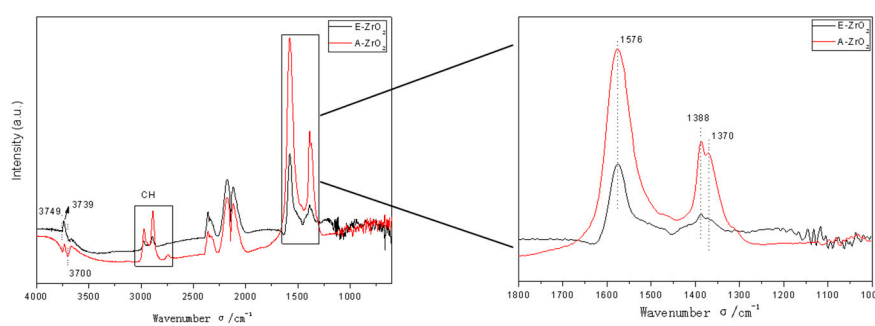


Figure 5. Infrared spectra of E, A-ZrO₂ catalysts exposed to CO.

Figure 6 shows infrared spectra recorded after CO saturated adsorption on the E-KCZ and A-KCZ catalysts. The results were the same as observed in Figure 5, with multicoordinated OH groups mainly consumed on E-ZrO₂, while different types of OH group were consumed on A-ZrO₂. In addition to CO₂ and CO gas, a new peak appeared at 2080 cm^{-1} that was attributed to linear CO adsorption on Cu⁰ [41,42]. Formate species (HCOO^-) were the main adsorption species owing to the bands at 2967 , 2870 , 1584 , 1386 , and 1369 cm^{-1} . Meanwhile, bicarbonate species (HCO_3^-) were also formed according to the bands at 1692 , 1644 , and 1280 cm^{-1} . In previous studies [43], bicarbonate species, as the precursors of formyl groups that participate in methanol and isobutanol formation, were found to be beneficial for isobutanol formation. The results showed that formate is mainly converted into methanol and methane, while bicarbonate is mainly converted into methane. Furthermore, formyl groups are converted into methyl groups after reaction, as discussed in previous studies regarding the isobutanol formation process. Therefore, the formed bicarbonate was assigned as an intermediate of isobutanol synthesis from syngas. A large amount of C₁ species (linear CO, HCOO^- , and HCO_3^-) were formed on A-KCZ compared with E-KCZ. Although bicarbonate species were formed on both types of catalyst, the selectivities for isobutanol were significantly different (Table 2). To obtain further information on the reaction, H₂/CO adsorption was investigated by in-situ DRIFTS at the reaction temperature (Figure 7). Compared with the results in Figures 5 and 6, the greatest difference was that formate species were the main adsorption species on the E-KCZ catalyst under a syngas atmosphere, while both formate and bicarbonate species were formed on the A-KCZ catalyst. This showed that bicarbonate species on the E-KCZ catalyst were not stable under a H₂/CO atmosphere. Based on the isobutanol formation mechanism (aldol condensation process), formyl species were the key intermediates in chain growth. Therefore, isobutanol formation was inhibited by the low bicarbonate species content (precursors of formyl species) on the E-KCZ catalyst.

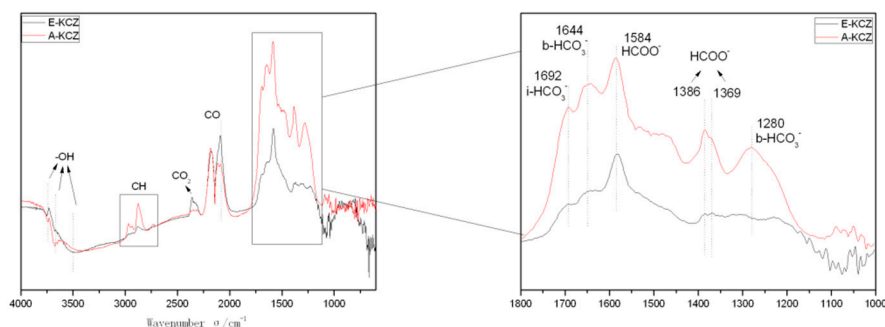


Figure 6. Infrared spectra of E, A-KCZ catalysts with CO adsorption.

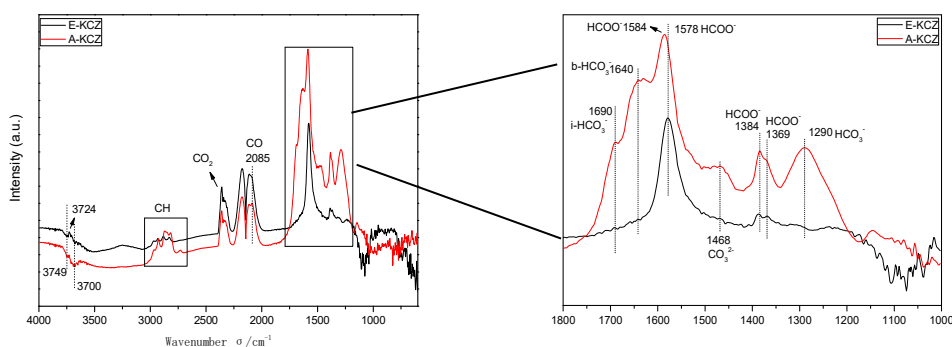


Figure 7. Infrared spectra of E, A-KCZ catalysts with H₂/CO adsorption.

Figures 6 and 7 show that bicarbonate species were formed on E-KCZ, but disappeared under a syngas atmosphere. To understand the factors influencing the stability of adsorbed species, H₂ was introduced to treating the surface species after saturated CO adsorption. Figure 8 shows the results of H₂ treatment after CO adsorption. Peaks related to bicarbonate species on the E-KCZ catalyst had nearly disappeared completely after H₂ introduction for 5 min. The intensity of peaks related to formate species also greatly decreased during the H₂-treatment process. The intensity of peaks related to formate and bicarbonate species on the A-KCZ catalyst obvious decreased after H₂ treatment for 5 min. Further treatment with H₂ led to a slight decrease in the peak intensity. Therefore, many bicarbonate species were still present on the A-KCZ catalyst, even after exposing to H₂ for 30 min. These results indicated that the stability of adsorption species on the A-ZrO₂ catalyst was relatively high compared with those adsorbed on the E-ZrO₂ catalyst. Formate species can also be reduced to formyl species by H₂, but preferentially form methanol owing to its weak adsorption intensity [44]. Intermediates with stronger adsorption intensities have relatively long residence times on the catalyst surface for further chain growth, leading to high selectivity for isobutanol.

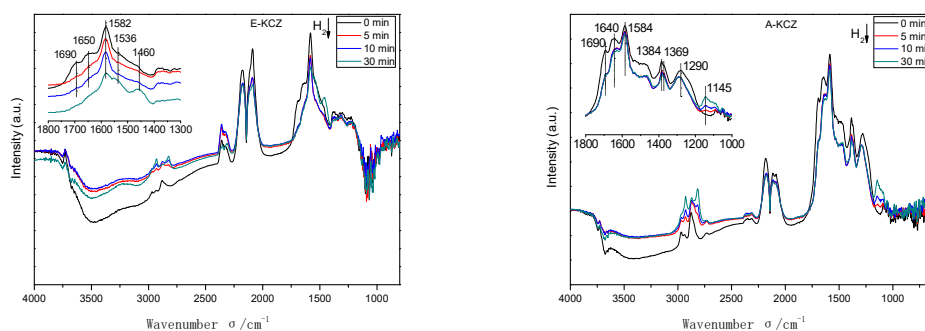


Figure 8. Infrared spectra of E, A-KCZ catalysts exposed to H₂ after CO adsorption.

3. Materials and Methods

3.1. Catalyst Preparation

An amorphous ZrO_2 type was prepared by precipitation followed by the reflux method, which was described in detail in the literature [22]. Firstly, $\text{ZrOCl}_2 \cdot 8\text{H}_2\text{O}$ was dissolved in deionized water under vigorous stirring. Then the ethylenediamine aqueous solution was added into mother liquor drop by drop until $\text{pH} = 11$. The obtained slurry was refluxed at $94\text{ }^\circ\text{C}$ for 40 h. After that, the precipitate was filtered and washed with deionized water to remove Cl^- , then followed by drying at $110\text{ }^\circ\text{C}$ for 12 h. Finally, the resulting product was calcined at $400\text{ }^\circ\text{C}$ for 4 h with a ramp of $2\text{ }^\circ\text{C}/\text{min}$ under static air. The obtained catalyst was named as E- ZrO_2 .

Another amorphous ZrO_2 type was prepared by a similar precipitation method as described above. The difference was that $\text{ZrO}(\text{NO}_3)_2 \cdot 2\text{H}_2\text{O}$ was introduced as the zirconium source and ammonia (30 wt%) was adopted as the precipitant. The obtained solution was digested at $94\text{ }^\circ\text{C}$ for 40 h and followed by the same processing method as described above. The obtained catalyst was named as A- ZrO_2 .

The K-Cu/ ZrO_2 catalysts were prepared by the incipient wetness impregnation method. An aqueous solution of $\text{Cu}(\text{NO}_3)_2 \cdot 3\text{H}_2\text{O}$ was added drop-wise to the ZrO_2 support to obtain 5 wt% Cu catalyst. The obtained material was dried at $110\text{ }^\circ\text{C}$ for 12 h and calcined at $400\text{ }^\circ\text{C}$ for 4 h. Then, 2 wt% K was introduced via the same impregnation method using KOH as precursor. The calcined powders promoted by Cu and K were marked as E-KCZ and A-KCZ respectively. Finally, all the catalysts were pressed and broken into 40–60 meshes in prior to reaction.

3.2. Catalyst Characterization

The specific surface areas (BET) and pore volumes of the samples were detected using Micromeritics Tristar 3000 instrument.

The X-ray diffraction (XRD) data of the calcined catalysts were obtained using a D8 Advance X-ray diffractometer (10° to 80°) with Cu $\text{K}\alpha$ radiation.

The temperature-programmed-reduction of H_2 (H_2 -TPR) profiles were recorded in an apparatus fed with a 10% H_2/Ar mixture flowing (30 mL/min) and rising rate of $10\text{ }^\circ\text{C}/\text{min}$. N_2O titration was used to determine the surface area of dispersed metallic copper (Cu^0) in the same TPR apparatus with a method described before [14].

The surface hydroxyl groups on different ZrO_2 -based catalysts were investigated under Ar flow on a Bruker Tensor 27 FT-IR spectrometer with a MCT detector ($4000\text{--}800\text{ cm}^{-1}$). The catalyst powder was put into the infrared cell with KBr window and scraped flat. Firstly, a background spectrum was recorded at the same conditions using KBr as reference substance. Then, the framework spectrum of the catalysts was obtained. All the catalysts were treated at $250\text{ }^\circ\text{C}$ for 1 h under high vacuum ($5.5 \times 10^{-2}\text{ Pa}$) for removing the surface adsorbed water.

In situ DRIFTS spectra were recorded on the same FT-IR spectrometer under atmospheric pressure. The catalysts were first reduced by pure H_2 at atmospheric pressure at $350\text{ }^\circ\text{C}$ for 2 h. Then, the H_2 flow was replaced by Ar for purging the chamber at $350\text{ }^\circ\text{C}$ for 30 min. After the background spectrum was collected under Ar flow at $350\text{ }^\circ\text{C}$, CO (15 mL/min) or H_2/CO ($v/v = 2.5/1$) mixture was introduced into the IR cell for obtaining the adsorption spectra. The Ar flow could be introduced into the chamber for detecting the stability of surface C_1 species.

3.3. Catalyst Evaluation

Higher alcohols were synthesized from syngas in a continuous flow via a high-pressure fixed-bed reactor. Before the reaction, 5 mL catalyst was reduced for 13 h under the designed temperature program ($25\text{ }^\circ\text{C}$ to $350\text{ }^\circ\text{C}$) at a flow rate of 20 mL/min in H_2/N_2 ($v/v = 10/90$). After reduction, the mixture of H_2/CO (2.5:1) was introduced into the reactor at a space velocity of 3000 h^{-1} . The reactions were conducted at $350\text{ }^\circ\text{C}$, 10 MPa, and the data was obtained after 8 h reaction. Gas chromatograph

(GC 4000) with flame ionization device (FID) and thermal conductivity detector (TCD) were used for on-line analysis of gas products. The detectors of FID and TCD use GDX-403 and carbon sieves columns, respectively. Then the composition of H₂, CH₄, CO, CO₂, and CH_x mixtures (C₁, C₂, C₃, C₄, and C₄₊) were analyzed. Liquid products were also detected by two sets of gas chromatography. Methanol and water were analyzed by GC 4000 (TCD) with a column of GDX-401 and the alcohol products were analyzed by GC-7A (FID) with a Chromosorb 101 column.

4. Conclusions

Two kinds of amorphous ZrO₂ (am-ZrO₂) were successfully synthesized by using different precipitation/reflux methods (with ethylenediamine and ammonia as the precipitant respectively). Copper and potassium were introduced for promoting ZrO₂ via a typical impregnation method, and then the obtained catalysts were evaluated in the isobutanol synthesis from syngas. These catalysts showed different catalytic performance under the same reaction conditions. In detail, methanol was the main alcohol product on both am-ZrO₂ catalysts. However, after promotion by Cu and K, the selectivity of isobutanol had an obvious increase. In the results, the selectivity of isobutanol on A-KCZ (ammonia as precipitant) was three times higher than that on E-KCZ (ethylenediamine as precipitant). Furthermore, the characterization results indicated that the kinds of hydroxyl groups on the two am-ZrO₂ catalysts were different. It not only had an important effect on the dispersion of Cu, but also possessed a significant influence in the contents and kinds of C₁ species formed on different catalysts. More isolated hydroxyls were formed on the A-KCZ catalyst surface, which were active for anchoring and dispersing Cu, at the same time as reacting with CO to form C₁ intermediates. In comparison, Cu species on the A-KCZ catalyst were well dispersed and had a strong interaction with ZrO₂, which led to a good catalytic performance for isobutanol synthesis. Meanwhile, more bicarbonate species related to isobutanol formation were formed after CO/H₂ adsorption on the A-KCZ surface, and these intermediates were very stable for further carbon chain growth process, leading to a high selectivity of isobutanol.

Author Contributions: The idea was conceived by L.T. and Y.W.; Y.W. performed the experiments and drafted the paper under the supervision of L.T.; T.Z., H.X., G.Y., N.T. and J.C. helped to collect and analyze some characterization data. The manuscript was revised and checked through the comments of all authors. All authors have given approval for the final version of the manuscript.

Funding: This research was funded by the Natural Science Foundation of China (21902029) and Open Subject Fund of State Key Laboratory of Coal Conversion (J19-20-612).

Acknowledgments: The authors thank the financial support of Natural Science Foundation of China (21902029) and Open Subject Fund of State Key Laboratory of Coal Conversion (J19-20-612).

Conflicts of Interest: The authors declare no conflict of interest.

References

1. Li, X.; Zhang, J.; Zhang, M.; Zhang, W.; Zhang, M.; Xie, H.; Wu, Y.; Tan, Y. The Support effects on the direct conversion of syngas to higher alcohol synthesis over copper-based catalysts. *Catalysts* **2019**, *9*, 199. [[CrossRef](#)]
2. Chen, T.; Su, J.; Zhang, Z.; Cao, C.; Wang, X.; Si, R.; Liu, X.; Shi, B.; Xu, J.; Han, Y. Structure Evolution of Co–CoO_x Interface for higher alcohol synthesis from syngas over Co/CeO₂ catalysts. *ACS Catal.* **2018**, *8*, 8606–8617. [[CrossRef](#)]
3. Sun, K.; Gao, X.; Bai, Y.; Tan, M.; Yang, G.; Tan, Y. Synergetic catalysis of bimetallic copper–cobalt nanosheets for direct synthesis of ethanol and higher alcohols from syngas. *Catal. Sci. Technol.* **2018**, *8*, 3936–3947. [[CrossRef](#)]
4. Luk, H.T.; Mondelli, C.; Mitchell, S.; Siol, S.; Stewart, J.A.; Ferré, D.C.; Pérez-Ramírez, J. Role of carbonaceous supports and potassium promoter on higher alcohols synthesis over copper–iron catalysts. *ACS Catal.* **2018**, *8*, 9604–9618. [[CrossRef](#)]
5. Ao, M.; Pham, G.H.; Sunarso, J.; Tade, M.O.; Liu, S. Active centers of catalysts for higher alcohol synthesis from syngas: A review. *ACS Catal.* **2018**, *8*, 7025–7050. [[CrossRef](#)]

6. Tian, S.; Wang, S.; Wu, Y.; Gao, J.; Bai, Y.; Wang, P.; Xie, H.; Han, Y.; Tan, Y. Cation distribution in Zn-Cr spinel structure and its effects on synthesis of isobutanol from syngas: Structure–activity relationship. *J. Mol. Catal. A Chem.* **2015**, *404*, 139–147. [[CrossRef](#)]
7. Tan, L.; Yang, G.; Yoneyama, Y.; Kou, Y.; Tan, Y.; Vitidsant, T.; Tsubaki, N. Iso-butanol direct synthesis from syngas over the alkali metals modified Cr/ZnO catalysts. *Appl. Catal. A Gen.* **2015**, *505*, 141–149. [[CrossRef](#)]
8. Gao, X.; Wu, Y.; Yang, G.; Zhang, T.; Li, X.; Xie, H.; Pan, J.; Tan, Y. Insight into the role of hydroxyl groups on the ZnCr catalyst for isobutanol. *Appl. Catal. A* **2017**, *547*, 1–11. [[CrossRef](#)]
9. Cheng, S.; Gao, Z.; Kou, J.; Liu, Y.; Huang, W. Direct synthesis of isobutanol from syngas over nanosized Cu/ZnO/Al₂O₃ catalysts derived from hydrotalcite-like materials supported on carbon fibers. *Energy Fuels* **2017**, *31*, 8572–8579. [[CrossRef](#)]
10. Li, X.; Xie, H.; Gao, X.; Wu, Y.; Wang, P.; Tian, S.; Zhang, T.; Tan, Y. Effects of calcination temperature on structure-activity of K-ZrO₂/Cu/Al₂O₃ catalysts for ethanol and isobutanol synthesis from CO hydrogenation. *Fuel* **2018**, *227*, 199–207. [[CrossRef](#)]
11. Kou, J.; Cheng, S.; Gao, Z.; Cheng, F.; Huang, W. Synergistic effects of potassium promoter and carbon fibers on direct synthesis of isobutanol from syngas over Cu/ZnO/Al₂O₃ catalysts obtained from hydrotalcite-like compounds. *Solid State Sci.* **2019**, *87*, 138–145. [[CrossRef](#)]
12. Cai, Y.; Niu, Y.; Chen, Z. Synthesis of methanol and isobutanol from syngas over ZrO₂-based catalysts. *Fuel Process. Technol.* **1997**, *50*, 163–170. [[CrossRef](#)]
13. He, D.; Ding, Y.; Luo, H.; Li, C. Effects of zirconia phase on the synthesis of higher alcohols over zirconia and modified zirconia. *J. Mol. Catal. A Chem.* **2004**, *208*, 267–271. [[CrossRef](#)]
14. Wu, Y.; Xie, H.; Tian, S.; Tsubaki, N.; Han, Y.; Tan, Y. Isobutanol synthesis from syngas over K–Cu/ZrO₂–La₂O₃(x) catalysts: Effect of La-loading. *J. Mol. Catal. A Chem.* **2015**, *396*, 254–260. [[CrossRef](#)]
15. Wang, J.; Tan, Y.; Niu, Y.; Zhong, B.; Peng, S. Relations between ZrO₂ crystal structure and its catalytic activity to methanol and isobutanol. *J. Fuel Chem. Technol.* **1998**, *26*, 390–394.
16. Rhodes, M.D.; Bell, A.T. The effects of zirconia morphology on methanol synthesis from CO and H₂ over Cu/ZrO₂ catalysts Part I. Steady-state studies. *J. Catal.* **2005**, *233*, 198–209. [[CrossRef](#)]
17. Aguila, G.; Guerrero, S.; Araya, P. Influence of the crystalline structure of ZrO₂ on the activity of Cu/ZrO₂ catalysts on the water gas shift reaction. *Catal. Commun.* **2008**, *9*, 2550–2554. [[CrossRef](#)]
18. Jackson, N.B.; Ekerdt, J.G. Methanol synthesis mechanism over zirconium dioxide. *J. Catal.* **1986**, *101*, 90–102. [[CrossRef](#)]
19. Tian, S.; Wang, S.; Wu, Y.; Gao, J.; Wang, P.; Xie, H.; Yang, G.; Han, Y.; Tan, Y. The role of potassium promoter in isobutanol synthesis over Zn–Cr based catalysts. *Catal. Sci. Technol.* **2016**, *6*, 4105–4115. [[CrossRef](#)]
20. Wu, Y.; Wang, S.; Xie, H.; Wang, J.; Tian, S.; Han, Y.; Tan, Y. Influence of Cu on the K-LaZrO₂ Catalyst for isobutanol synthesis. *Acta Phys.-Chim. Sin.* **2015**, *31*, 166–172. [[CrossRef](#)]
21. Deshmane, V.G.; Adewuyi, Y.G. Synthesis of thermally stable, high surface area, nanocrystalline mesoporous tetragonal zirconium dioxide (ZrO₂): Effects of different process parameters. *Micropor. Mesopor. Mater.* **2012**, *148*, 88–100. [[CrossRef](#)]
22. Atzori, L.; Rombi, E.; Meloni, D.; Sini, M.F.; Monaci, R.; Cutrufello, M.G. CO and CO₂ co-methanation on Ni/CeO₂-ZrO₂ soft-templated catalysts. *Catalysts* **2019**, *9*, 415. [[CrossRef](#)]
23. Shimokawabe, M.; Asakawa, H.; Takezawa, N. Characterization of copper zirconia catalysts prepared by an impregnation method. *Appl. Catal.* **1990**, *59*, 45–58. [[CrossRef](#)]
24. Zhou, R.; Yu, T.; Jiang, X.; Chen, F.; Zheng, X. Temperature-programmed reduction and temperature-programmed desorption studies of CuO/ZrO₂ catalysts. *Appl. Surf. Sci.* **1999**, *148*, 263–270. [[CrossRef](#)]
25. Chen, C.; Ruan, C.; Zhan, Y.; Lin, X.; Zheng, Q.; Wei, K. The significant role of oxygen vacancy in Cu/ZrO₂ catalyst for enhancing water-gas-shift performance. *Int. J. Hydrogen Energy* **2014**, *39*, 317–324. [[CrossRef](#)]
26. Kondo, J.; Sakata, Y.; Domen, K.; Maruya, K.; Onishi, T. Infrared study of hydrogen adsorbed on ZrO₂. *J. Chem. Soc. Faraday Trans.* **1990**, *86*, 397–401. [[CrossRef](#)]
27. Zhang, X.; Shi, H.; Xu, B. Vital roles of hydroxyl groups and gold oxidation states in Au/ZrO₂ catalysts for 1,3-butadiene hydrogenation. *J. Catal.* **2011**, *279*, 75–87. [[CrossRef](#)]
28. Graf, P.O.; de Vlieger, D.J.M.; Mojet, B.L.; Lefferts, L. New insights in reactivity of hydroxyl groups in water gas shift reaction on Pt/ZrO₂. *J. Catal.* **2009**, *262*, 181–187. [[CrossRef](#)]

29. Karwacki, C.J.; Ganesh, P.; Kent, P.R.C.; Gordon, W.O.; Peterson, G.W.; Niu, J.J.; Gogotsi, Y. Structure-activity relationship of Au/ZrO₂ catalyst on formation of hydroxyl groups and its influence on CO oxidation. *J. Mater. Chem. A* **2013**, *1*, 6051–6062. [[CrossRef](#)]
30. Bianchi, D.; Gass, J.L.; Khalfallah, M.; Teichner, S.J. Intermediate species on zirconia supported methanol aerogel catalysts. 1. State of the catalyst surface before and after the adsorption of hydrogen. *Appl. Catal. A Gen.* **1993**, *101*, 297–315. [[CrossRef](#)]
31. Binet, C.; Daturi, M.; Lavalley, J.C. IR study of polycrystalline ceria properties in oxidised and reduced states. *Catal. Today* **1999**, *50*, 207–225. [[CrossRef](#)]
32. Köck, E.M.; Kogler, M.; Bielz, T.; Klötzer, B.; Penner, S. In situ FT-IR spectroscopic study of CO₂ and CO adsorption on Y₂O₃, ZrO₂, and Yttria-stabilized ZrO₂. *J. Phys. Chem. C* **2013**, *117*, 17666–17673. [[CrossRef](#)]
33. Chen, H.; Zhang, X.; Wang, Q. Hydroconversion of C₁₈ fatty acids using PtNi/Al₂O₃: Insight in the role of hydroxyl groups in Al₂O₃. *Catal. Commun.* **2017**, *97*, 14–17. [[CrossRef](#)]
34. Namiki, T.; Yamashita, S.; Tominaga, H.; Nagai, M. Dissociation of CO and H₂O during water–gas shift reaction on carburized Mo/Al₂O₃ catalyst. *Appl. Catal. A Gen.* **2011**, *398*, 155–160. [[CrossRef](#)]
35. Wang, X.; Shi, H.; Kwak, J.H.; Szanyi, J. Mechanism of CO₂ Hydrogenation on Pd/Al₂O₃ catalysts: Kinetics and transient DRIFTS-MS studies. *ACS Catal.* **2015**, *5*, 6337–6349. [[CrossRef](#)]
36. Quiroz, J.; Giraudon, J.M.; Gervasini, A.; Dujardin, C.; Lancelot, C.; Trentesaux, M.; Lamonier, J.F. Total oxidation of formaldehyde over MnO_x-CeO₂ catalysts: The effect of acid treatment. *ACS Catal.* **2015**, *5*, 2260–2269. [[CrossRef](#)]
37. Zhang, T.; Wu, Y.; Gao, X.; Xie, H.; Yang, G.; Tsubaki, N.; Tan, Y. Effects of surface hydroxyl groups induced by the co-precipitation temperature on the catalytic performance of direct synthesis of isobutanol from syngas. *Fuel* **2019**, *237*, 1021–1028. [[CrossRef](#)]
38. Yang, R.; Fu, Y.; Zhang, Y.; Xu, B.; Tsubaki, N. In-situ DRIFT study of a low-temperature methanol synthesis mechanism on Cu/ZnO catalysts from CO₂-containing syngas using ethanol promoter. *J. Catal.* **2004**, *228*, 23–35. [[CrossRef](#)]
39. Kiss, J.; Frenzel, J.; Meyer, B.; Marx, D. Methanol synthesis on ZnO(0001). II. Structure, energetics, and vibrational signature of reaction intermediates. *J. Chem. Phys.* **2013**, *139*, 1–17. [[CrossRef](#)]
40. Sanchez-Escribano, V.; Larrubia Vargas, M.A.; Finocchio, E.; Busca, G. On the mechanisms and the selectivity determining steps in syngas conversion over supported metal catalysts: An IR study. *Appl. Catal. A Gen.* **2007**, *316*, 68–74. [[CrossRef](#)]
41. Sun, Q.; Liu, C.W.; Pan, W.; Zhu, Q.M.; Deng, J.F. In situ IR studies on the mechanism of methanol synthesis over an ultrafine Cu/ZnO/Al₂O₃ catalyst. *Appl. Catal. A Gen.* **1998**, *171*, 301–308. [[CrossRef](#)]
42. Peltier, F.L.; Chaumette, P.; Saussey, J.; Bettaha, M.M.; Lavalley, J.C. In-situ FT-IR spectroscopy and kinetic study of methanol synthesis from CO/H₂ over ZnAl₂O₄ and Cu-ZnAl₂O₄ catalysts. *J. Mol. Catal. A* **1997**, *122*, 131–139. [[CrossRef](#)]
43. Wu, Y.; Gong, N.; Zhang, M.; Zhang, W.; Zhang, T.; Zhang, J.; Wang, L.; Xie, H.; Tan, Y. Insight into the branched alcohols formation mechanism on KZnCr catalysts from syngas. *Catal. Sci. Technol.* **2019**, *9*, 2592–2600. [[CrossRef](#)]
44. Wu, Y.; Zhang, J.; Zhang, T.; Sun, K.; Wang, L.; Xie, H.; Tan, Y. Effect of potassium on the regulation of C₁ intermediates in isobutyl alcohol synthesis from syngas over CuLaZrO₂ catalysts. *Ind. Eng. Chem. Res.* **2019**, *58*, 9343–9351. [[CrossRef](#)]

